Published in final edited form as:
Biochim Biophys Acta. 2013 June ; 1828(6): 1432–1440. doi:10.1016/j.bbamem.2013.02.006.

Properties of Membranes Derived from the Total Lipids Extracted from the Human Lens Cortex and Nucleus

Laxman Mainali[a,1], **Marija Raguz**[a,1,c], **William J. O'Brien**[b,1], and **Witold K. Subczynski**[a,1,*]

[a]Department of Biophysics, Milwaukee, WI 53226, USA

[b]Department of Ophthalmology and Microbiology/Molecular Genetics, Milwaukee, WI 53226, USA

[1]Medical College of Wisconsin, Milwaukee, WI 53226, USA

[c]Department of Medical Physics and Biophysics, School of Medicine, University of Split, Split, Croatia

Abstract

Human lens lipid membranes prepared using a rapid solvent exchange method from the total lipids extracted from the clear lens cortex and nucleus of 41- to 60-year-old donors were investigated using electron paramagnetic resonance spin-labeling. Profiles of the phospholipid alkyl-chain order, fluidity, oxygen transport parameter, and hydrophobicity were assessed across coexisting membrane domains. Membranes prepared from the lens cortex and nucleus were found to contain two distinct lipid environments, the *bulk phospholipid-cholesterol domain* and the *cholesterol bilayer domain* (CBD). The alkyl chains of phospholipids were strongly ordered at all depths, indicating that the amplitude of the wobbling motion of alkyl chains was small. However, profiles of the membrane fluidity, which explicitly contain time (expressed as the spin-lattice relaxation rate) and depend on the rotational motion of spin labels, show relatively high fluidity of alkyl chains close to the membrane center. Profiles of the oxygen transport parameter and hydrophobicity have a rectangular shape and also indicate a high fluidity and hydrophobicity of the membrane center. The amount of CBD was greater in nuclear membranes than in cortical membranes. The presence of the CBD in lens lipid membranes, which at 37°C showed a permeability coefficient for oxygen about 60% smaller than across a water layer of the same thickness, would be expected to raise the barrier for oxygen transport across the fiber cell membrane. Properties of human membranes are compared with those obtained for membranes made of lipids extracted from cortex and nucleus of porcine and bovine eye lenses.

Keywords

cholesterol; membrane domains; fluidity; hydrophobic barrier; oxygen permeation; EPR; spin labeling

*Corresponding Author: Witold K. Subczynski, Department of Biophysics, Medical College of Wisconsin, 8701 Watertown Plank Road, Milwaukee, WI 53226, USA. Tel: (414) 955-4038; Fax: (414) 955-6512; subczyn@mcw.edu.

1. Introduction

The fiber cell plasma membrane is a structure that can affect the function of the entire eye lens. Its properties are largely determined by two components: (1) membrane proteins (which allow communication between layers of fiber cells) and (2) the lipid bilayer portion of the membrane (which determines bulk membrane properties, including diffusion barriers, and may also affect the properties of membrane proteins) [1, 2]. Previously, we successfully applied electron paramagnetic resonance (EPR) spin-labeling methods to study the properties of the lipid bilayer portion of bovine and porcine lens membranes. First, we studied lens lipid membranes (without proteins) made of the total lipids extracted from fiber cell plasma membranes [3, 4], as well as lipid membranes prepared from lipids extracted from the cortical and nuclear regions of the eye lens [5, 6]. Second, we examined intact fiber cell plasma membranes (containing proteins) isolated from the cortical and nuclear regions of the porcine lens [7]. Maturation of fiber cells results in a loss of cellular organelles [8–10]. Thus, the plasma membrane essentially becomes the only membranous structure of the cell [11]. The goal of the presented research is to study the properties of human lens lipid membranes made from the total lipids extracted from the cortical and nuclear regions of the clear human eye lenses of 41- to 60-year-old donors. This research is important for further studies of membranes from clear human lens of different age groups and membranes from cataractous human lenses.

The plasma membrane of the human fiber cell has a unique molecular composition, with an extremely high level of cholesterol [12–14]. A Cholesterol-to-phospholipid (Chol/PL) molar ratio from 1 to 2 is shown in the cortex and a ratio as high as 4 is present in the lens nucleus. It also has been found that during aging the Chol/PL ratio increases [12–14]. At an elevated Chol concentration, the entire membrane become saturated with Chol and is in the liquid-ordered-like phase (organized like a raft [2]). It has also been hypothesized that under these conditions Chol forms immiscible cholesterol bilayer domains (CBDs) within the bulk membrane [1, 15]. It is understood that these domains play a positive physiological role in the eye, maintaining lens transparency to visible light [15–18].

Human lens fiber cell membranes also show an extremely high content of sphingomyelins (SM) [19–21]. For 70-year-old donors, they account for two-thirds of membrane PLs [22]. Phosphatidylcholine (PC) is the major PL in the lens membranes of animals with short life spans, while SM is the predominant PL in the lens membranes of animals (including humans) with long life spans [22, 23]. Changes that occur with age in the human lens include depletion of glycerophospholipids and increased amounts of SMs, with preferential enlargement in dihydro-SM [1]. A high content of saturated sphingolipids [19–21], and only traces of polyunsaturated fatty acids [24, 25], ensure physical [3, 23] and chemical [26] stability (rigidity and resistance to peroxidation) of the membrane. Age-related changes in lipid composition are reflected in regional differences in the fiber cell membrane [17, 27]. Specifically, there is a higher Chol/PL molar ratio in the nucleus than in the cortex [5, 28–31]. Nuclear membranes contain more sphingolipids than cortical [1]. The amount of proteins in fiber cell plasma membranes increases with age. Therefore, intact nuclear membranes are also denser in proteins than cortical membranes [17].

Such great variation in PL composition and Chol content with age and lens region suggests that unique mechanisms exist to maintain homeostasis in the fiber cell membrane. This observation is especially significant for humans. Humans have the longest life span, and changes in their lens lipid composition with age are the most pronounced [1, 12, 13, 27]. We cannot assume that the properties of animal lens lipid membranes (isolated from animals two-year-old or younger) described previously [3–6] can properly reflect the properties of human lens lipid membranes from adult donors. Thus, we presented results about properties

of human lens lipid membranes obtained using EPR spectroscopy with PL and Chol analogue spin labels (see Fig. 1 in Ref. [7] for their structures). Additionally, in the presented investigations, the rapid solvent exchange method was used for preparation of human lens lipid membranes. This method is preferable to the film deposition method we previously used. At a high Chol content in the lipid mixture (which is the case for lipid extracts from the human lens cortex and nucleus), and during membrane preparation using the film deposition method, the lipid mixture passes through the solid-state intermediate, at which point solid-state demixing of Chol can occur. This can produce lower Chol content in the PL bilayer because Chol trapped in these solid-state structures (Chol crystals) do not participate in further liposome formation [32]. We also applied a new EPR spin-labeling method to study profiles of membrane fluidity as compared with previous studies. This new T_1-sensitive EPR spin-labeling method is described in recent papers [33, 34].

2. Materials and Methods

2.1. Materials

One-palmitoyl-2-(*n*-doxylstearoyl)phosphatidylcholine (*n*-PC, $n = 5, 7, 10, 12, 14$, or 16) and tempocholine-1-palmitoyl-2-oleoylphosphatidic acid ester (T-PC) spin labels were obtained from Avanti Polar Lipids, Inc. (Alabaster, AL). Cholesterol analogues (androstane spin label [ASL] and cholestane spin label [CSL]) and 9-doxylstearic acid spin labels (9-SASL) were purchased from Molecular Probes (Eugene, OR). (See Fig. 1 in [7] for spin-label structures.) Other chemicals of at least reagent grade were purchased from Sigma-Aldrich (St. Louis, MO).

2.2. Isolation of total lipids from the cortical and nuclear fiber-cell membranes of human eye lenses and analysis of lipid composition

Fifty clear human lenses were obtained from the Lions Eye Bank of Wisconsin. Lens sample donors ranged in age from 41 to 60 years. Lenses were removed *in situ* from refrigerated bodies within an average time frame of nine hours postmortem. All of the lenses were stored at −80°C until lipid isolations were performed. Fifty lenses were accumulated over four months, and then the lipid isolations were performed. The cortical and nuclear regions of the lenses were separated based on differences in tissue consistency [28, 35]. The total lipids from the cortical or nuclear samples were extracted separately based on minor modifications of the Folch procedure [36]. Details of these procedures were described earlier [6]. The resultant lipid samples were soft, white solids and were stored at −20°C.

The samples were sent to Avanti Polar Lipids (Alabaster, AL) for analysis of the total lipid extract using the high-performance liquid chromatography. Results for the cortex and nucleus samples, respectively, are as follows: 1.38 and 2.1 for Chol/PL, 0.22 and 0.21 for PC/PL, 0.59 and 0.61 for SM/PL, 0.08 and 0.06 for PS/PL, and 0.10 and 0.11 for PE/PL. Values of the Chol/PL molar ratios in our samples are close to the values reported earlier for the pools of human lenses ranging from 13 to 68 years old: 2.6 for cortical and 3.2 for nuclear membranes [31]. Values of 1.4 for cortical and of 2.4 for nuclear membranes were also reported [24]. A value of 3.0 was reported for membranes prepared from whole lens [25]. However, there is evidence that multilamellar bodies of the fiber cell cytoplasm contain Chol [37, 38] what can affect (increase) the Chol/PL molar ratio in membranes calculated based on the total lipid extraction. The relative abundance of phospholipid classes (PC, phosphatidylcholine; SM, sphingomyelin plus dihydrosphingomyelin; PS, phosphatidylserine; PE, phosphatidylethanolamine) is close to the amount reported in [22].

2.3. Preparation of samples for EPR measurements

The membranes were prepared using the rapid solvent exchange method [32, 39, 40] with the apparatus that was recently built in our lab, as described in detail in [39]. This preparation forms probably multilamellar liposomes, but it was not checked here. This improved design increased solvent-removal efficiency twofold. A chloroform solution of lens lipids with a final volume of 75 μL was added at room temperature to the 1.2 mL of buffer (10 mM PIPES and 150 mM NaCl, pH 7.0) in a test tube. As described [39], the tube was mounted on a laboratory vortexer and coupled to the sample manifold of the rapid solvent exchange device. The vortexer was actuated, the flushing-argon flow rate was confirmed, and the manifold valve was quickly opened to a trap-protected vacuum system preset at ~25 torr. After the appropriate time elapsed, the vortexer was stopped, the manifold was vented, and the sample tube was removed from the device. The membrane suspensions were then used for EPR experiments. As was indicated in [39] the 100 s was enough time to remove chloroform from samples. To ensure that all chloroform was removed, we kept samples under the reduced pressure for four minutes, which caused reduction of the buffer volume to 1.0 mL. Although, we made all possible effort to completely remove chloroform from our samples, the amount of solvent left in the lipids investigated was not checked. Thus, we cannot completely neglect the case that a residual solvent may modify membrane properties.

For EPR measurements the membrane suspensions (containing 1 to 2 mg/mL of total lipids to which ~1 mol% spin label (*n*-PC, T-PC, 9-SASL, ASL, or CSL) was added) were centrifuged briefly (12000g, 15 min, 4°C), and the loose pellet (~20% lipid, wt/wt) was transferred to a 0.6 mm i.d. capillary made of gas-permeable methylpentene polymer (TPX) and used for EPR measurements [41]. Each membrane sample was prepared from stock solutions. EPR measurements were completed on the same day.

2.4. EPR measurements

To further increase the signal-to-noise ratio, samples were centrifuged in TPX capillaries as described in [41]. Conventional EPR spectra were recorded with a Bruker EMX spectrometer equipped with temperature-control accessories. All spectra were obtained at 37°C with a modulation amplitude of 1.0 G and an incident microwave power of 5.0 mW. Samples were thoroughly deoxygenated, yielding correct EPR lineshapes. To assess the order parameter, $A'_{\|}$ and $A'_{\perp}$ values were measured directly from the EPR spectra, as indicated in Fig. 1A. The order parameter was calculated, as described in detail in Ref. [42].

Due to the sharpness of the EPR lines and the method of measurement, $A'_{\|}$ and $A'_{\perp}$ values could be measured with an accuracy of ±0.1 G, and the order parameter could be evaluated with an accuracy of ±0.015. To measure hydrophobicity, the *z*-component of the hyperfine interaction tensor of *n*-PC or 9-SASL, A_Z, was determined from the EPR spectra (as indicated in Fig. 5A) for samples frozen at −165°C, and recorded with a modulation amplitude of 2.0 G and an incident microwave power of 2.0 mW [43]. Values of $2A_Z$ were measured with an accuracy of ±0.25 G.

Spin-lattice relaxation times, T_1s, of spin labels were determined by analyzing the saturation recovery (SR) signal of the central line obtained by short-pulse SR EPR at X-band [44–46]. Accumulation of the decay signals were carried out with 2048 data points on each decay. T_1s of spin labels (membrane fluidity) were determined, as indicated in Fig. 2A, for thoroughly deoxygenated samples [33]. For measurements of the oxygen transport parameter (Figs. 3A, 4A and C), the sample was equilibrated with the same gas used for temperature control (*i.e.*, a controlled mixture of nitrogen and dry air adjusted with flowmeters [Matheson Gas Products, model 7631H-604]) [41, 47, 48]. For measurements of

the NiEDDA accessibility parameter (Fig. 4B and D), a 20 mM NiEDDA was present in the buffer and SR measurements were performed for deoxygenated samples [49, 50]. SR signals were fitted by single- or double-exponential functions. The standard deviations in the measurements of decay time from the fits were usually less than 0.05%. However, the decay times determined from sample to sample were with an accuracy of ±3% when a single-exponential fit was satisfactory and with an accuracy of less than ±5% and ±10% for longer and shorter recovery time constants, respectively, when a double-exponential fit was satisfactory.

3. Results and Discussion

PL and Chol analogue spin labels are incorporated in the membrane with the nitroxide moiety located at specific depths and in specific membrane domains. These spin labels should approximate Chol–PL and Chol–Chol interactions in the membrane as well as be distributed between different membrane domains similarly to parent molecules [3–5]. A schematic drawing that shows possible cases of spin-label distribution that may be relevant to eye-lens-lipid membranes are shown in Fig. 2 of Ref. [2]. In membranes oversaturated with Chol, in which CBDs are formed (which is the case for human lens lipid membranes), the PL analogue spin labels should partition only into the bulk PL-Chol domain, and the Chol analogues should be distributed between the two domains. Thus, only Chol analogue spin labels can discriminate the two coexisting domains (Sect. 3. 3). However, the unique distribution of PL analogue spin labels allows profiles of the order parameter and fluidity (Sect. 3.1), oxygen transport parameter (Sect. 3.2), and hydrophobicity (Sect. 3.4) to be obtained in the bulk PL-Chol domain without “contamination” from the CBD.

3.1. Order and fluidity of phospholipid alkyl chains

In *n*-PC spin labels, the nitroxide moiety is rigidly attached to the C_n carbon of the alkyl chain of the PL molecule. Therefore, the order parameter extracted from the conventional EPR spectra (Fig. 1A) and the dynamic parameter (spin-lattice relaxation rate) extracted from the saturation-recovery signals (Fig. 2A) reflect the order and dynamics of the rigid alkyl chain fragment C_{n-1}–C_n–C_{n+1}. The order parameter, which describes the amplitude of the wobbling motion of the alkyl chain fragment, has been routinely used as a measure of membrane fluidity [51–55]. However, this parameter does not explicitly contain time or velocity and therefore can be considered non-dynamic. The spin-lattice relaxation rate (T_1^{-1}) obtained from SR EPR measurements of lipid spin labels in deoxygenated samples depends primarily on the rotational correlation time of the nitroxide moiety within the lipid bilayer [56, 57]. Thus, T_1^{-1} can be used as a convenient quantitative measure of membrane fluidity that reflects local motional properties of the lipid alkyl chain [6, 33, 34, 58, 59]. Here, for the first time we have used both displays as a convenient quantitative measure of the alkyl chain order and the rate of alkyl-chain motion of *n*-PC and 9-SASL in the cortical and nuclear lens lipid membranes.

Figure 1A shows representative conventional EPR spectra of 5- and 16-PC in cortical membranes. The values used for the calculation of the alkyl chain order parameter [42], $A'_{\|}$ and $A'_{\perp}$, are measured directly from the spectra as shown in the figure. Figure 1B shows profiles of the order parameter across the PL bilayer portion of cortical and nuclear lens lipid membranes. Both profiles have an inverted bell-shape and show that alkyl-chain order gradually decreases with depth in the membrane. Although the PL composition of the cortical and nuclear membranes differs significantly (see Sect. 2.2), both profiles are practically identical. These profiles are also very similar to those across porcine and bovine lens lipid membranes [5, 6], which have very different PL compositions than human membranes [22]. Values of the order parameter measured at all depths in human (Fig. 1B)

and in animal lens lipid membranes [3–5, 7] are significantly greater than those measured for membranes without Chol [2–5, 58, 59]. Thus, the ordering effect of Chol on alkyl chains is observed at all depths, from the membrane surface to the membrane center.

Results obtained are in principal agreement with two previous papers showing that the structural order (the static value of the *trans*/*gauche* rotamer ratio in the hydrocarbon chains) in human lens lipids did not differ between the human cortex and nucleus [60, 61]. Borchman et al. [62] reported also that the structural order of the bovine cortical and nuclear lens lipid membranes are similar when the nuclear lipids contain 59 mol% Chol, while cortical lipids contain only 36 mol% Chol. They suggested that PL composition affects the Chol concentration, at which the structural orders of cortical and nuclear membranes are similar.

Figure 2A shows representative SR signals of 5-PC and 16-PC in deoxygenated cortical lens lipid membranes. SR measurements were carried out systematically as a function of the location of the nitroxide moiety of spin labels in the membrane. SR signals for 5-PC and 16-PC were fitted successfully to a single-exponential function, indicating that the environment sensed by these spin labels is homogenous. Similarly, single-exponential curves were good fits for other *n*-PC spin labels and 9-SASL both in deoxygenated cortical and nuclear lens lipid membranes (data not shown). Fluidity profiles (T_1^{-1} versus depth in the membrane) are presented in Fig. 2B. As expected, membrane fluidity (dynamics of PL alkyl chains) increases toward the center of both membranes (which is indicated by an increase in T_1^{-1}). Similarly to profiles of the order parameter fluidity profiles in cortical and nuclear lens lipid membranes are practically identical. Thus, the extremely high (saturating) content of Chol, and not the PL composition, determines the order and fluidity of PL alkyl chains (but see the discussion in Sect. 3.5 about the interplay between the CBD and the surrounding bulk PL-Chol domain).

In previously published studies [6, 58, 59], we have shown, using the dynamic parameter T_1^{-1}, that Chol has a rigidifying effect on alkyl chains only to the depth occupied by the rigid steroid-ring structure. At deeper locations within the membrane, Chol has a fluidizing effect. For the same samples, profiles of the order parameter show that Chol has an ordering effect on alkyl chains at all depths. In quaternary PL mixtures, resembling composition of human lenses [22], Chol decreases membrane dynamics (T_1^{-1} values of PL spin labels) to the depth of C9, and increases membrane dynamics at deeper locations. However, the ordering effect of Chol was observed at all depths (data not shown, but see Fig 5C and F in [2]). Similar results were also reported for ternary mixtures of SM, PC, and Chol, showing that in the membrane center Chol can increase alkyl chain order and at the same time increase the rate of alkyl chain rotational motion [63]. All this data suggests that in human lens lipid membranes Chol decreases membrane dynamics to a depth to which the rigid ring structure of Chol is immersed in the membrane, while the mobility of alkyl chains is enhanced at deeper locations.

Explanation is needed to clarify the seeming conflict between the well-established condensing effect of Chol (manifesting itself by the ordering of alkyl chains), which extend to the whole alkyl chain of the lipid bilayer [51–53, 64, 65] and the Chol effect on membrane dynamics, which is suppressed only to the depth of the C9 and increased at deeper locations [33, 34, 46]. Deviations of the alkyl chain segment direction from the bilayer normal accumulate as one proceeds from the bilayer surface to the membrane center, a result of the effective tethering of the alkyl chain at the bilayer surface. Thus, ordering of the alkyl chain induced by the steric contact with the plate-like ring structure of Chol will also cause ordering of the distal fragment of the alkyl chain, even though free volume in the membrane center is created because the isooctyl chain of Chol has a cross-section much

smaller than that across the Chol ring structure. This free volume, however, provides an additional opportunity for *gauche-trans* isomerization of the alkyl chains of neighboring PLs, and thus facilitates the rate of motion in that region (see also discussion in [46]).

3.2. Membrane fluidity reported in terms of translational diffusion of molecular oxygen

In another approach, membrane organization and fluidity is reported on the movement of molecular oxygen within the membrane, but not directly on the motion and organization of alkyl chains. Here, the observable parameter is the spin-lattice relaxation time (T_1) of spin labels, and the measured value is the bimolecular collision rate between molecular oxygen and the nitroxide moiety of spin labels (the oxygen transport parameter) [45, 48]. Profiles of membrane fluidity obtained by these methods differ drastically from typical profiles of membrane fluidity reported by alkyl chain order and dynamics [58]. The oxygen transport parameter reveals more features and possesses much greater spatial sensitivity (in some cases can differentiate the effect of Chol at atomic resolution [3]).

Figure 3A shows representative SR signals of 5-PC and 16-PC in deoxygenated nuclear lens lipid membranes and membranes equilibrated with 50% air at 37°C. All SR signals were fitted successfully to single-exponential functions. SR measurements were carried out systematically for all PL analogue spin labels as a function of the partial pressure of oxygen in the equilibrating gas mixture, and single-exponential recovery was consistently observed. This indicates that the bulk PL-Chol domain in cortical and nuclear lens lipid membranes is homogenous (see also [58] for more detail).

Profiles of the oxygen transport parameter across the bulk PL-Chol domain of cortical and nuclear lens lipid membranes are presented in Fig. 3B. They have a rectangular shape with an abrupt increase in the oxygen transport parameter between the C9 and C10 positions. This abrupt increase is as large as 3 times, and the overall change of the oxygen transport parameter across the membrane becomes as large as 8 times. The oxygen transport parameter from the membrane surface to the depth of the C9 was as low as in gel-phase PC membranes, and at locations deeper than the C9, as high as in fluid-phase membranes [45, 66]. Similarly to profiles of the order parameter and the spin-lattice relaxation rate, profiles of the oxygen transport parameter in cortical and nuclear lens lipid membranes are practically identical. They are also practically identical to those across porcine and bovine lens lipid membranes [5, 6].

These profiles are typical for liquid-ordered-phase membranes saturated with Chol and are very different from the bell-shaped profile across model membranes without Chol [3–5, 58, 59] and across liquid-ordered-phase raft domains containing ~30 mol% Chol (the minimal concentration of Chol in liquid-ordered-phase membranes) [67]. All these indicate that the bulk PL-Chol portion of lens lipid membranes possess unique properties. As was shown previously [66], oxygen transport parameter strongly depends on the rate of *gauche-trans* isomerization of lipid alkyl chains. According to the proposed model of oxygen transport in the membrane, molecular oxygen enters transient small vacant pockets created by *gauche-trans* isomerization of alkyl chains or by the structural non-conformability of neighboring molecules (mismatch in surface topography of molecules when two molecules are placed side by side in the membrane), and oxygen molecule jump from one pocket to an adjacent one or move along with the movement of the pocket itself [66, 68–70]. It follows that the alkyl chains and the rigid plate-like ring structure of Chol are well packed, with few vacant pockets to even allow entrance and movement of small molecules such as molecular oxygen and/or the *gauche-trans* isomerization in this membrane region is as slow as in the gel-phase membranes. The opposite situation is in the membrane center. Free volume created because of the difference in cross-section of Chol ring structure and its isooctyl chain enhances not only alkyl chain dynamics but also concentration and diffusion of small molecules. The

oxygen transport parameter measured in the membrane center can be even greater than in membranes without Chol (see Fig 6 in [7]).

3.3. Discrimination of membrane domains using cholesterol-analogue spin labels

Because of the high Chol content and the new method of liposome preparation (the rapid solvent exchange method), we expected that the CBD would be detected using Chol analogue spin labels in both cortical and nuclear human lens lipid membranes. Figure 4 shows representative SR signals of ASL in the presence and absence of oxygen (A,C) and CSL in the presence and absence of NiEDDA (B,D) in cortical (A,B) and nuclear (C,D) lens lipid membranes. The single-exponential fits were satisfactory for both ASL and CSL in cortical and nuclear membranes in the absence of relaxation agents. For ASL in the presence of oxygen, the single-exponential fits were not satisfactory, while the double-exponential fits were excellent (compare residuals for single- and double-exponential fits in Figs. 4A and C). T_1 values from double-exponential curves allowed us to calculate the oxygen transport parameter in the bulk PL-Chol domain and in the CBD (see Refs. [4, 5, 50] for details of assigning SR data to a certain domain). All SR signals obtained with CSL in the presence of oxygen were single exponentials (data not shown). Because CSL should also be distributed between both domains, we conclude that the collision rate between oxygen and the nitroxide moiety of CSL (oxygen transport parameter) is the same in the PL-Chol domain and the CBD (see also the discussion in Ref. [4]). Values of the oxygen transport parameter in discriminated domains are collected in the Table 1.

The water-soluble relaxation agent, NiEDDA, should strongly affect the T_1 values of CSL, the spin labels with the nitroxide moiety at the membrane-water interface. Figures 4B and D show representative SR signals for CSL in the presence and absence of NiEDDA in cortical and nuclear lens lipid membranes. In the presence of NiEDDA, single-exponential fits were not satisfactory, while double-exponential fits were excellent (compare the residual for single- and double-exponential fits in Figs. 4B and D). T_1 values from double-exponential curves allowed us to calculate the NiEDDA accessibility parameter in coexisting membrane domains and assigned them to the bulk PL-Chol domain (the smaller values) and to the CBD (the greater values) (see also Refs. [4, 5, 50] for detail of assigning SR data to a certain domain). All SR signals obtained with ASL in the presence of NiEDDA were single-exponentials, with the time constant nearly the same as in the absence of NiEDDA (data not shown). It was confirmed that NiEDDA does not penetrate the membrane center where the nitroxide moiety of ASL is located. Values of the NiEDDA accessibility parameter in discriminated domains are collected in the Table 1. Thus, the existence of the CBD in cortical and nuclear lens lipid membranes was confirmed using ASL and oxygen as a relaxation agent and CSL and NiEDDA as a relaxation agent.

The pre-exponential factors in the fitting of the double-exponential SR curves should indicate a population of ASL or CSL in the CBD and the bulk PL-Chol domain and thus should directly report on the amount of Chol in coexisting domains. These factors were obtained from double-exponential saturation-recovery curves in the presence of 50% air (for ASL) and 20 mM NiEDDA (for CSL) in cortical and nuclear lens lipid membranes. The pre-exponential factors that indicate the population of ASL in the CBD and the PL-Chol domain are 0.14 and 0.86 for cortical and 0.26 and 0.74 for nuclear membranes. Similarly, pre-exponential factors indicating the population of CSL in the CBD and the PL-Chol domain are 0.25 and 0.75 for cortical and 0.37 and 0.63 for nuclear membranes. Thus, the amount of Chol involved in the formation of the CBD is greater in nuclear membranes than in cortical membranes. This can be the result of the higher Chol content in nuclear membranes as comparable with that in cortical membranes (but see the discussion below).

The CBD is observed in cortical and nuclear human lens lipid membranes from 41- to 60-year-old donors, while it was observed only in nuclear lens lipid membranes of two-year-old porcine and bovine [5, 6]. Chol content in cortical human lens lipid membranes is higher compared with that in the cortex of porcine and bovine eye lenses, which should explain this result. However, in simple binary mixtures of PLs and Chol, the minimal Chol concentration at which the CBD starts to be formed depends on the kind of PL. In 1-palmitoyl-2-oleoylphosphatidylserine (POPS) membranes, the CBD is formed at Chol/POPS molar ratios exceeding 0.5 [50]; in 1-palmitoyl-2-oleoylphosphatidylcholine (POPC) membranes, at Chol/POPC molar ratios exceeding 1 [49]; and in SM membranes, at Chol/SM molar ratios equal to or exceeding 2 [71]. Based on these data we hypothesized [2] that the PL composition of the lens lipid membrane can determine the Chol concentration at which the CBD is formed. Thus, the delicate balance between changes in the lens membrane PL composition and changes in the Chol content controls the formation of the CBD.

3.4. Hydrophobicity of membrane interior

The EPR spin-labeling method allows hydrophobicity profiles across lipid bilayer membranes to be obtained. In these profiles, $2A_Z$ values (measured directly from EPR spectra as shown in Fig. 5A) are plotted as a function of the position of the nitroxide moiety of the spin label within the lipid bilayer. With an increase in hydrophobicity around the nitroxide moiety, the $2A_Z$ value decreases (see Fig. 1 in Ref. [43]). Thus, changes in spectra between 5-PC and 16-PC (Fig. 5A) indicate that the membrane interior is more hydrophobic than the hydrocarbon region close to the membrane surface. Figure 5B shows hydrophobicity profiles across the bulk PL-Chol domain of cortical and nuclear lens lipid membranes. In both membranes, hydrophobicity profiles show similar rectangular shapes, with an abrupt increase of hydrophobicity between C9 and C10. The $2A_Z$ values in the center of both membranes (positions of 10-, 12-, 14-, and 16-PC) indicate that hydrophobicity in this region can be compared to that of hexane and dipropylamine (ε = 2.0–2.9), and hydrophobicity near the membrane surface (positions of 5- and 7-PC) can be compared to that of methanol and ethanol (ε = 24.3–32.6), although this is still considerably less polar than the bulk aqueous phase (ε = 80). We relate the local hydrophobicity as observed by $2A_Z$ to the hydrophobicity (or ε) of the bulk organic solvent by referring to Fig. 2 in Ref. [43].

The rectangular hydrophobicity profile is characteristic for PL membranes saturated with Chol where the abrupt increase in hydrophobicity occurs between C9 and C10 [2–6, 58, 59]. Interestingly, when membranes contain lower Chol concentration (30 mol%), the abrupt increase occurs between C7 and C9 for saturated membranes and membranes containing *trans* double bonds, and between C9 and C10 for unsaturated membranes containing *cis* double bonds [43]. Lens lipid membranes are saturated with Chol and contain mostly saturated alkyl chains. For all these membranes made from lipids isolated from eye lenses of different species the abrupt increase of hydrophobicity was always observed between C9 and C10 positions. Also all these membranes show similar, high hydrophobicity in the membrane center (ε = 2.0–2.9). However, the hydrophobicity to the depth of C9 differs from species to species and is higher in cortical than in nuclear membranes [5, 7].

High Chol content is responsible for the formation of the hydrophobic barrier in human cortical and nuclear lens lipid membranes. The high hydrophobic barrier is located in the membrane center. This barrier ensures that the transport of water, ions, and other small polar and ionic molecules is tightly controlled by membrane proteins, which allow communication between layers of fiber cells [72, 73].

3.5. Permeability of oxygen across membrane domains

For further processing of our data, we included oxygen transport parameter values obtained with ASL and CSL into the profiles presented in Fig. 3B. As can be seen, one of the two oxygen transport parameter values obtained with ASL fits satisfactorily into the profile across the PL-Chol domain, which also confirms correct assignment of the SR data. The other value indicates the oxygen transport parameter in the CBD. As explained in Sect. 3.3, values of the oxygen transport parameter obtained with CSL are the same in the bulk PL-Chol domain and the CBD. These data allowed us to draw approximate profiles of the oxygen transport parameter across the CBD of cortical and nuclear membranes (Fig. 3B). Based on these profiles and the method of evaluating the membrane permeability coefficient for oxygen (for details, see the Sect. Calculation of the membrane oxygen permeability coefficient in Supporting Material), we evaluated the permeability coefficient for oxygen across coexisting bulk PL-Chol domains and the CBDs in human cortical and nuclear lens lipid membranes (Table 2). Values are similar to those obtained earlier for these domains in porcine and bovine lens lipid membranes [4, 5, 7, 74]. The permeability coefficient for oxygen across the CBD formed in human cortical and nuclear lens lipid membranes is also close to what was previously reported across the CBD formed in porcine and bovine lens lipid membranes and in simple model membranes [4, 5]. There is an interesting interplay between the CBD and the surrounding bulk PL-Chol domain in lens lipid membranes. The CBD provides a buffering capacity for Chol concentration in the surrounding PL bilayer, keeping it at a constant saturating level. However, the PL composition of the lens lipid membrane determines the maximal solubility of Chol in the PL environment and therefore controls the Chol/PL molar ratio at which the pure CBDs begin to form. This mechanism through which Chol-dependent processes in the eye lens could be regulated is discussed in Rev. [2].

Even though the CBD is a pure Chol bilayer, its properties can be affected by the size of the domain. For small CBDs, Chol exchange between the CBD and the surrounding bulk PL-Chol domain (where the oxygen transport parameter is significantly greater) was expected to result in an increased permeability coefficient for oxygen. This was the case for simple model membranes with Chol concentrations only slightly exceeding the concentration necessary for formation of the CBD [2, 4, 59]. At high Chol contents, the permeability coefficient for oxygen across the CBD remained at minimal value, similar to that reported for the CBD in human nuclear lens lipid membranes (Table 2). Thus, the greater permeability coefficient for oxygen across the CBD in cortical lens lipid membranes (Table 2) suggests that the size of CBDs in cortical membranes is smaller than that in nuclear membranes.

A moderately low and low permeability coefficient for oxygen across the bulk PL-Chol domain and the CBD, respectively (Table 2) supports our conclusion that the lipid bilayer portion of the fiber-cell plasma membrane can form a barrier for oxygen transport into the lens interior. High barriers formed by the membranes of fiber cells can help maintain a low oxygen partial pressure in the lens nucleus even at a very low oxygen consumption rate. It should be stressed that oxygen must pass through thousands of fiber cell membranes on its way from the lens surface to its center and a very small oxygen concentration difference across each membrane can significantly contribute to the oxygen concentration gradient across the eye lens (see also Rev. [2] where these problems are discussed in more details).

4. Concluding Remarks

We presented detailed profiles across domains in cortical and nuclear human lens lipid membranes made of lipids extracted from clear lenses of 41- to 60-year old donors. This age group contains already-matured lens fiber cells with well-separated cortical and nuclear

regions, but lenses are not yet affected by age. Thus, these profiles should form good starting points for further research on lenses from different age groups and on cataractous lenses. Compared with our previous studies on animal lens lipid membranes, we introduce new profiles of membrane fluidity, namely, profiles of the spin-lattice relaxation rate, which provide information about the rate of motion of alkyl chains of PLs. This allowed us to conclude that alkyl chains are fairly fluid in the central region of lens lipid membranes. These unique properties of PL-Chol domains in lens lipid membranes are determined by the saturating amount of Chol.

Although our obtained profiles are very similar to those presented earlier for porcine and bovine lens lipid membranes, the human lens lipid membranes acquired had drastically different PL compositions. The results further support our statement that the saturating amount of Chol is the major factor that determines the bulk properties of the PL-Chol membranes, while the PL composition controls the Chol/PL molar ratio at which the membrane becomes saturated with Chol (at which CBDs begin to form) [2].

Supplementary Material

Refer to Web version on PubMed Central for supplementary material.

Acknowledgments

This work was supported by grants EY015526, EB002052, EB001980, EY001931, and a construction grant, RR016511, from the National Institutes of Health. We thank Dr. Jeffrey T. Buboltz at University of Wisconsin-Platteville for his help in building the rapid solvent exchange device and helpful discussions.

References

1. Borchman D, Yappert MC. Lipids and the ocular lens. J Lipid Res. 2010; 51:2473–2488. [PubMed: 20407021]
2. Subczynski WK, Raguz M, Widomska J, Mainali L, Konovalov A. Functions of cholesterol and the cholesterol bilayer domain specific to the fiber-cell plasma membrane of the eye lens. The Journal of membrane biology. 2012; 245:51–68. [PubMed: 22207480]
3. Widomska J, Raguz M, Dillon J, Gaillard ER, Subczynski WK. Physical properties of the lipid bilayer membrane made of calf lens lipids: EPR spin labeling studies. Biochim Biophys Acta. 2007; 1768:1454–1465. [PubMed: 17451639]
4. Raguz M, Widomska J, Dillon J, Gaillard ER, Subczynski WK. Characterization of lipid domains in reconstituted porcine lens membranes using EPR spin-labeling approaches. Biochim Biophys Acta. 2008; 1778:1079–1090. [PubMed: 18298944]
5. Raguz M, Widomska J, Dillon J, Gaillard ER, Subczynski WK. Physical properties of the lipid bilayer membrane made of cortical and nuclear bovine lens lipids: EPR spin-labeling studies. Biochim Biophys Acta. 2009; 1788:2380–2388. [PubMed: 19761756]
6. Mainali L, Raguz M, Camenisch TG, Hyde JS, Subczynski WK. Spin-label saturation-recovery EPR at W-band: Applications to eye lens lipid membranes. J Magn Reson. 2011; 212:86–94. [PubMed: 21745756]
7. Mainali L, Raguz M, O'Brien WJ, Subczynski WK. Properties of fiber cell plasma membranes isolated from the cortex and nucleus of the porcine eye lens. Experimental eye research. 2012; 97:117–129. [PubMed: 22326289]
8. Bassnett S. Lens organelle degradation. Experimental eye research. 2002; 74:1–6. [PubMed: 11878813]
9. Bassnett S, Beebe DC. Coincident loss of mitochondria and nuclei during lens fiber cell differentiation. Developmental dynamics : an official publication of the American Association of Anatomists. 1992; 194:85–93. [PubMed: 1421526]

10. Wride MA. Lens fibre cell differentiation and organelle loss: many paths lead to clarity, Philosophical transactions of the Royal Society of London. Series B. Biological sciences. 2011; 366:1219–1233. [PubMed: 21402582]
11. Beebe, DC. The lens. In: Kaufman, PL., editor. Physiology of the eye. Mosby-Year Book; St Louis: 2003. p. 117-158.
12. Li LK, So L, Spector A. Membrane cholesterol and phospholipid in consecutive concentric sections of human lenses. J Lipid Res. 1985; 26:600–609. [PubMed: 4020298]
13. Li LK, So L, Spector A. Age-dependent changes in the distribution and concentration of human lens cholesterol and phospholipids. Biochim Biophys Acta. 1987; 917:112–120. [PubMed: 3790601]
14. Truscott RJ. Age-related nuclear cataract: a lens transport problem. Ophthalmic research. 2000; 32:185–194. [PubMed: 10971179]
15. Mason R, Tulenko TN, Jacob RF. Direct evidence for cholesterol crystalline domains in biological membranes: role in human pathobiology. Biochim Biophys Acta. 2003; 1610:198–207. [PubMed: 12648774]
16. Bach D, Wachtel E. Phospholipid/cholesterol model membranes: formation of cholesterol crystallites. Biochim Biophys Acta. 2003; 1610:187–197. [PubMed: 12648773]
17. Jacob RF, Cenedella RJ, Mason RP. Direct evidence for immiscible cholesterol domains in human ocular lens fiber cell plasma membranes. The Journal of biological chemistry. 1999; 274:31613–31618. [PubMed: 10531368]
18. Jacob RF, Cenedella RJ, Mason RP. Evidence for distinct cholesterol domains in fiber cell membranes from cataractous human lenses. The Journal of biological chemistry. 2001; 276:13573–13578. [PubMed: 11278611]
19. Byrdwell WC, Borchman D. Liquid chromatography/mass-spectrometric characterization of sphingomyelin and dihydrosphingomyelin of human lens membranes. Ophthalmic research. 1997; 29:191–206. [PubMed: 9261843]
20. Byrdwell WC, Borchman D, Porter RA, Taylor KG, Yappert MC. Separation and characterization of the unknown phospholipid in human lens membranes. Investigative ophthalmology & visual science. 1994; 35:4333–4343. [PubMed: 8002253]
21. Huang L, Grami V, Marrero Y, Tang D, Yappert MC, Rasi V, Borchman D. Human lens phospholipid changes with age and cataract. Investigative ophthalmology & visual science. 2005; 46:1682–1689. [PubMed: 15851569]
22. Deeley JM, Mitchell TW, Wei X, Korth J, Nealon JR, Blanksby SJ, Truscott RJ. Human lens lipids differ markedly from those of commonly used experimental animals. Biochim Biophys Acta. 2008; 1781:288–298. [PubMed: 18474264]
23. Borchman D, Yappert MC, Afzal M. Lens lipids and maximum lifespan. Experimental eye research. 2004; 79:761–768. [PubMed: 15642313]
24. Broekhuyse RM, Soeting WJ. Lipids in tissues of the eye. XV. Essential fatty acids in lens lipids. Experimental eye research. 1976; 22:653–657. [PubMed: 776644]
25. Zelenka PS. Phospholipid composition and metabolism in the embryonic chicken lens. Experimental eye research. 1978; 26:267–274. [PubMed: 639879]
26. Huang L, Estrada R, Yappert MC, Borchman D. Oxidation-induced changes in human lens epithelial cells. 1. Phospholipids. Free Radic Biol Med. 2006; 41:1425–1432. [PubMed: 17023269]
27. Yappert MC, Rujoi M, Borchman D, Vorobyov I, Estrada R. Glycero- versus sphingo-phospholipids: correlations with human and non-human mammalian lens growth. Experimental eye research. 2003; 76:725–734. [PubMed: 12742355]
28. Rujoi M, Jin J, Borchman D, Tang D, Yappert MC. Isolation and lipid characterization of cholesterol-enriched fractions in cortical and nuclear human lens fibers. Investigative ophthalmology & visual science. 2003; 44:1634–1642. [PubMed: 12657603]
29. Fleschner CR, Cenedella RJ. Lipid composition of lens plasma membrane fractions enriched in fiber junctions. J Lipid Res. 1991; 32:45–53. [PubMed: 2010693]
30. Li LK, So L. Age dependent lipid and protein changes in individual bovine lenses. Current eye research. 1987; 6:599–605. [PubMed: 3581878]

31. Borchman D, Delamere NA, Cauley LA, Paterson CA. Studies on the distribution of cholesterol, phospholipid and protein in the human and bovine lens. Lens Eye Ex Res. 1989; 6:703–724.
32. Huang J, Buboltz JT, Feigenson GW. Maximum solubility of cholesterol in phosphatidylcholine and phosphatidylethanolamine bilayers. Biochim Biophys Acta. 1999; 1417:89–100. [PubMed: 10076038]
33. Mainali L, Feix JB, Hyde JS, Subczynski WK. Membrane fluidity profiles as deduced by saturation-recovery EPR measurements of spin-lattice relaxation times of spin labels. J Magn Reson. 2011; 212:418–425. [PubMed: 21868272]
34. Mainali L, Hyde JS, Subczynski WK. Using spin-label W-band EPR to study membrane fluidity profiles in samples of small volume. J Magn Reson. 2013; 226:35–44. [PubMed: 23207176]
35. Estrada R, Yappert MC. Regional phospholipid analysis of porcine lens membranes by matrix-assisted laser desorption/ionization time-of-flight mass spectrometry. J Mass Spectrom. 2004; 39:1531–1540. [PubMed: 15578747]
36. Folch J, Lees M, Sloane Stanley GH. A simple method for the isolation and purification of total lipids from animal tissues. The Journal of biological chemistry. 1957; 226:497–509. [PubMed: 13428781]
37. VanMarle J, Vrensen GFJM. Cholesterol Content of Focal Opacities and Multilamellar Bodies in the Human Lens: Filipin Cytochemistry and Freeze Fracture. Ophthalmic research. 2000; 32:285–291. [PubMed: 11015040]
38. Duindam JJ, Vrensen GF, Otto C, Greve J. Cholesterol, phospholipid, and protein changes in focal opacities in the human eye lens. Investigative ophthalmology & visual science. 1998; 39:94–103. [PubMed: 9430550]
39. Buboltz JT. A more efficient device for preparing model-membrane liposomes by the rapid solvent exchange method. Rev Sci Instrum. 2009; 80:124301. [PubMed: 20059155]
40. Buboltz JT, Feigenson GW. A novel strategy for the preparation of liposomes: rapid solvent exchange. Biochimica et Biophysica Acta. 1999; 1417:232–245. [PubMed: 10082799]
41. Subczynski WK, Felix CC, Klug CS, Hyde JS. Concentration by centrifugation for gas exchange EPR oximetry measurements with loop-gap resonators. Journal of magnetic resonance. 2005; 176:244–248. [PubMed: 16040261]
42. Marsh, D. Electron spin resonance: spin labels. In: Grell, E., editor. Membrane Spectroscopy. Springer-Verlag; Berlin: 1981. p. 51-142.
43. Subczynski WK, Wisniewska A, Yin JJ, Hyde JS, Kusumi A. Hydrophobic barriers of lipid bilayer membranes formed by reduction of water penetration by alkyl chain unsaturation and cholesterol. Biochemistry. 1994; 33:7670–7681. [PubMed: 8011634]
44. Kawasaki K, Yin JJ, Subczynski WK, Hyde JS, Kusumi A. Pulse EPR detection of lipid exchange between protein rich raft and bulk domains in the membrane: methodology development and its application to studies of influenza viral membrane. Biophysical journal. 2001; 80:738–748. [PubMed: 11159441]
45. Subczynski WK, Hyde JS, Kusumi A. Oxygen permeability of phosphatidylcholine-cholesterol membranes. Proceedings of the National Academy of Sciences of the United States of America. 1989; 86:4474–4478. [PubMed: 2543978]
46. Yin JJ, Subczynski WK. Effects of lutein and cholesterol on alkyl chain bending in lipid bilayers: a pulse electron spin resonance spin labeling study. Biophysical journal. 1996; 71:832–839. [PubMed: 8842221]
47. Subczynski WK, Hopwood LE, Hyde JS. Is the mammalian cell plasma membrane a barrier to oxygen transport? The Journal of general physiology. 1992; 100:69–87. [PubMed: 1324973]
48. Kusumi A, Subczynski WK, Hyde JS. Oxygen transport parameter in membranes as deduced by saturation recovery measurements of spin-lattice relaxation times of spin labels. Proceedings of the National Academy of Sciences of the United States of America. 1982; 79:1854–1858. [PubMed: 6952236]
49. Raguz M, Mainali L, Widomska J, Subczynski WK. Using spin-label electron paramagnetic resonance (EPR) to discriminate and characterize the cholesterol bilayer domain. Chemistry and physics of lipids. 2011; 164:819–829. [PubMed: 21855534]

50. Raguz M, Mainali L, Widomska J, Subczynski WK. The immiscible cholesterol bilayer domain exists as an integral part of phospholipid bilayer membranes. Biochim Biophys Acta. 2011; 1808:1072–1080. [PubMed: 21192917]
51. Shin YK, Freed JH. Dynamic imaging of lateral diffusion by electron spin resonance and study of rotational dynamics in model membranes. Effect of cholesterol. Biophysical journal. 1989; 55:537–550. [PubMed: 2539210]
52. Quinn PJ, Wolf C. The liquid-ordered phase in membranes. Biochimica et biophysica acta. 2009; 1788:33–46. [PubMed: 18775411]
53. Hung WC, Lee MT, Chen FY, Huang HW. The condensing effect of cholesterol in lipid bilayers. Biophysical journal. 2007; 92:3960–3967. [PubMed: 17369407]
54. Devaux, PF. ESR and NMR Studies of Lipid-Protein Interactions in Membranes. In: Berliner, LJ.; Reuben, J., editors. Biological Magnetic Resonance. Plenum Press; New York: 1983. p. 183-299.
55. Schreier S, Polnaszek CF, Smith IC. Spin labels in membranes. Problems in practice. Biochim Biophys Acta. 1978; 515:395–436. [PubMed: 215206]
56. Robinson BH, Haas DA, Mailer C. Molecular dynamics in liquids: spin-lattice relaxation of nitroxide spin labels. Science (New York, NY. 1994; 263:490–493.
57. Mailer C, Nielsen RD, Robinson BH. Explanation of spin-lattice relaxation rates of spin labels obtained with multifrequency saturation recovery EPR. J Phys Chem A. 2005; 109:4049–4061. [PubMed: 16833727]
58. Subczynski WK, Raguz M, Widomska J. Studying lipid organization in biological membranes using liposomes and EPR spin labeling. Methods Mol Biol. 2010; 606:247–269. [PubMed: 20013402]
59. Mainali L, Raguz M, Subczynski WK. Phases and domains in sphingomyelin-cholesterol membranes: structure and properties using EPR spin-labeling methods. European biophysics journal : EBJ. 2012; 41:147–159. [PubMed: 22033879]
60. Borchman D, Lamba OP, Yappert MC. Structural characterization of lipid membranes from clear and cataractous human lenses. Experimental eye research. 1993; 57:199–208. [PubMed: 8405186]
61. Borchman D, Ozaki Y, Lamba OP, Byrdwell WC, Yappert MC. Age and regional structural characterisation of clear human lens lipid membranes by infrared and near-infrared Raman spectroscopy. Biospectroscopy. 1996; 2:113–123.
62. Borchman D, Cenedella RJ, Lamba OP. Role of cholesterol in the structural order of lens membrane lipids. Experimental eye research. 1996; 62:191–197. [PubMed: 8698079]
63. Smith AK, Freed JH. Dynamics and ordering of lipid spin-labels along the coexistence curve of two membrane phases: an ESR study. Chemistry and physics of lipids. 2012; 165:348–361. [PubMed: 22586732]
64. Stockton GW, Smith IC. A deuterium nuclear magnetic resonance study of the condensing effect of cholesterol on egg phosphatidylcholine bilayer membranes. I. Perdeuterated fatty acid probes. Chem Phys Lipids. 1976; 17:251–263. [PubMed: 1033045]
65. Rog T, Pasenkiewicz-Gierula M, Vattulainen I, Karttunen M. Ordering effects of cholesterol and its analogues. Biochim Biophys Acta. 2009; 1788:97–121. [PubMed: 18823938]
66. Subczynski WK, Hyde JS, Kusumi A. Effect of alkyl chain unsaturation and cholesterol intercalation on oxygen transport in membranes: a pulse ESR spin labeling study. Biochemistry. 1991; 30:8578–8590. [PubMed: 1653601]
67. Subczynski WK, Wisniewska A, Hyde JS, Kusumi A. Three-dimensional dynamic structure of the liquid-ordered domain as examined by a pulse-EPR oxygen probing. Biophysical journal. 2007; 92:1573–1584. [PubMed: 17142270]
68. Trauble H. The movement of molecules across lipid membranes: A molecular theory. J Membr Biol. 1971; 4:193–208.
69. Pace RJ, Chan SI. Molecular motions in lipid bilayers. III. Lateral and transverse diffusion in bilayers. J Chem Phys. 1982; 76:4241–4247.
70. Haines TH, Liebovitch L. P-lipid lateral diffusion, water transport and the order parameter: a molecular model of water transport through bilayers. Biophys J. 1993:A184.

71. Mainali L, Raguz M, Subczynski WK. Phase-Separation and Domain-Formation in Cholesterol-Sphingomyelin Mixture: Pulse-EPR Oxygen Probing. Biophysical journal. 2011; 101:837–846. [PubMed: 21843474]

72. Bassnett S, Shi Y, Vrensen GF. Biological glass: structural determinants of eye lens transparency, Philosophical transactions of the Royal Society of London. Series B. Biological sciences. 2011; 366:1250–1264. [PubMed: 21402584]

73. Dahm R, van Marle J, Quinlan RA, Prescott AR, Vrensen GF. Homeostasis in the vertebrate lens: mechanisms of solute exchange, Philosophical transactions of the Royal Society of London. Series B. Biological sciences. 2011; 366:1265–1277. [PubMed: 21402585]

74. Widomska J, Raguz M, Subczynski WK. Oxygen permeability of the lipid bilayer membrane made of calf lens lipids. Biochim Biophys Acta. 2007; 1768:2635–2645. [PubMed: 17662231]

Highlights

- Physical properties of human cortical and nuclear lens lipid membranes
- Discriminated domains are phospholipid cholesterol and cholesterol bilayer domains
- Presence of the cholesterol bilayer domain raise the barrier for oxygen transport

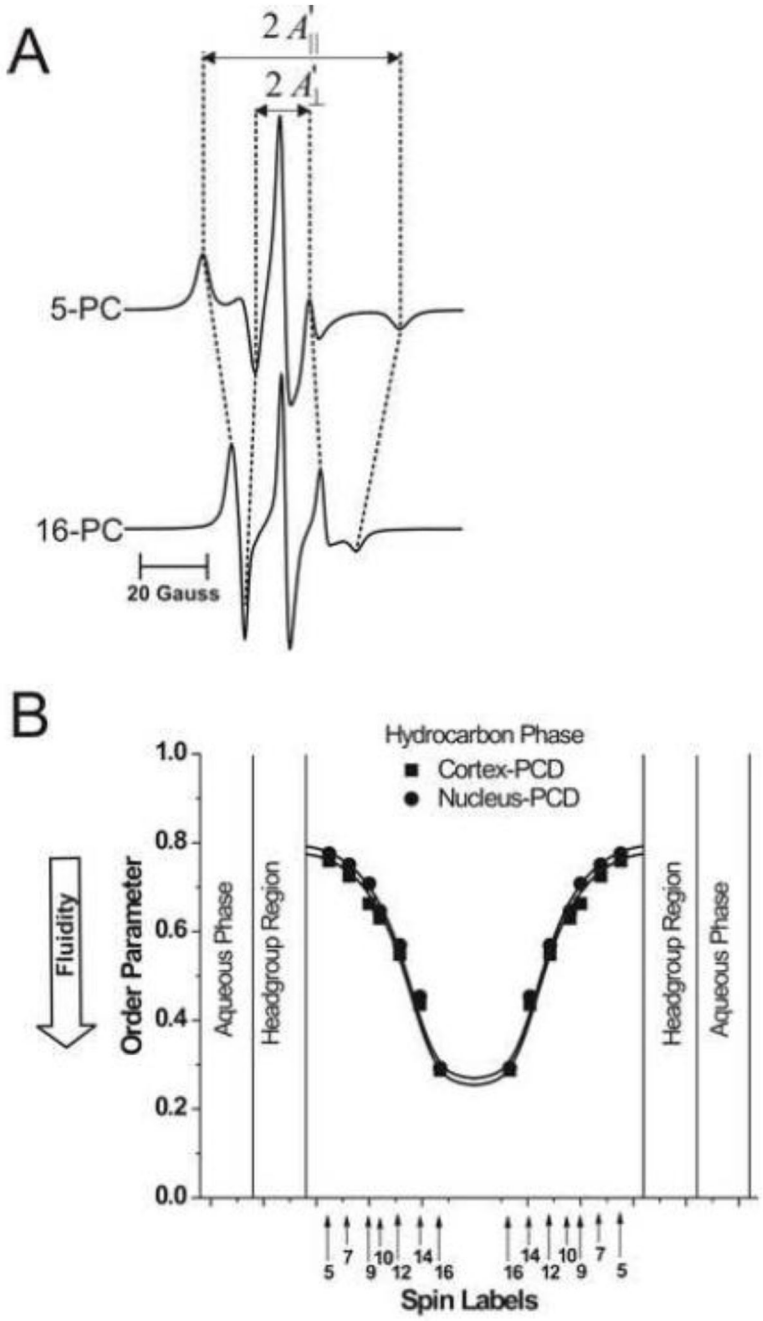

Fig. 1.

(A) Representative EPR spectra of 5- and 16-PC from cortical lens lipid membranes. Spectra were recorded at 37°C. Measured values used to calculate the order parameter are indicated. The positions of certain peaks were evaluated with a high level of accuracy. They were monitored at a receiver gain ten times higher and, when necessary, a higher modulation amplitude. (B) Profiles of the order parameter were obtained with *n*-PCs at 37°C for cortical and nuclear lens lipid membranes (PCD, phospholipid-cholesterol domain). Approximate localizations of the nitroxide moieties of spin labels are indicated by arrows.

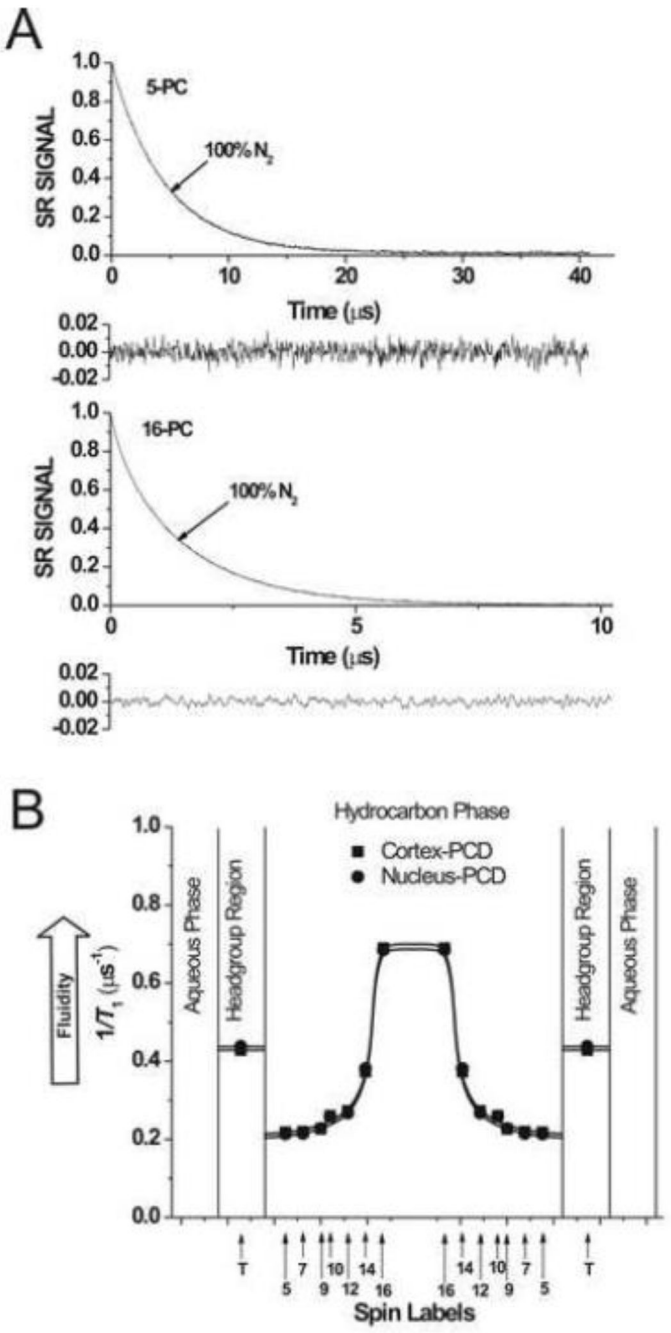

Fig. 2.

(A) Representative SR signals with fitted curves and residuals (the experimental signal minus the fitted curve) of 5- and 16-PC from cortical lens lipid membranes. Signals were recorded for deoxygenated samples (equilibrated with 100% nitrogen). The SR signals can be satisfactorily fitted with a single exponential function: for 5-PC, with a time constant of 4.58 ± 0.01 μs, and for 16-PC, with a time constant of 1.45 ± 0.01 μs (see residuals). (B) Profiles of T_1^{-1} (the spin-lattice relaxation rate) obtained for *n*-PC spin labels at 37°C for cortical and nuclear lens lipid membranes (PCD, phospholipid-cholesterol domain). Approximate localizations of the nitroxide moieties of spin labels are indicated by arrows.

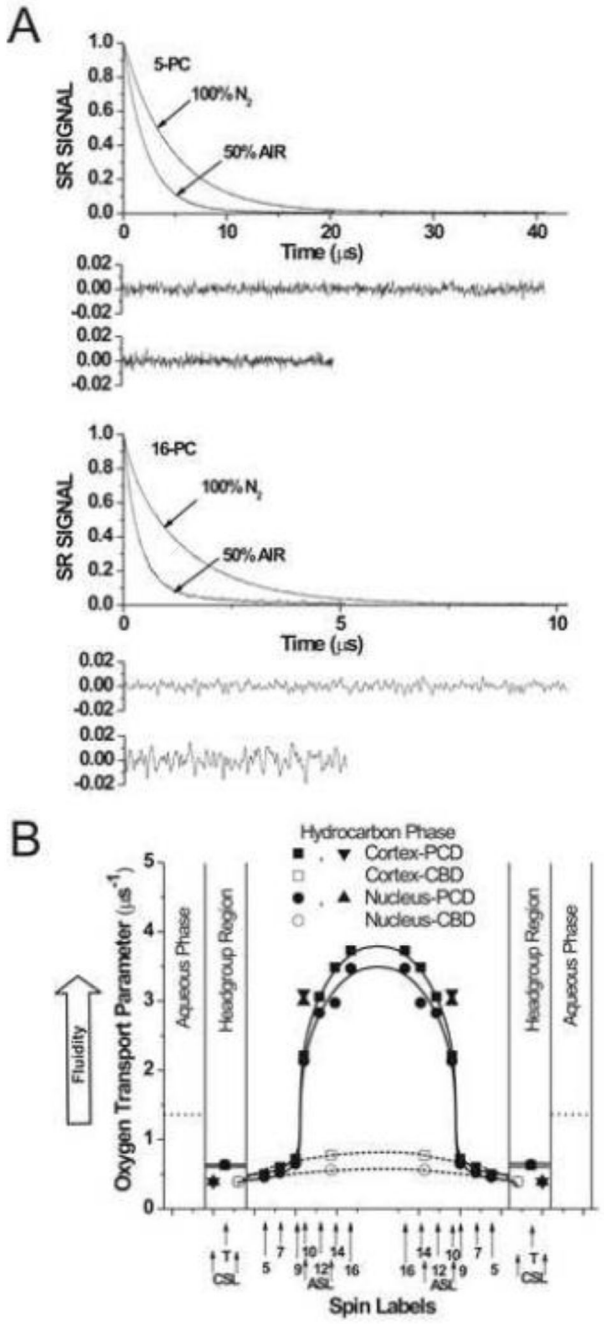

Fig. 3.

A) Representative SR signals with fitted curves and residuals (the experimental signal minus the fitted curve) of 5-PC and 16-PC from nuclear lens lipid membranes. Signals were recorded for samples equilibrated with 100% nitrogen and a gas mixture of 50% air/50% nitrogen. All SR signals can be satisfactorily fitted with a single exponential function: for 5-PC, with time constants of 4.67 ± 0.01 μs and 2.24 ± 0.1 μs, respectively; for deoxygenated samples and samples equilibrated with 50% air and for 16-PC, with time constants of 1.46 ± 0.01 μs and 0.42 ± 0.01 μs, respectively; for deoxygenated samples and samples equilibrated with 50% air (see residuals, upper residuals are for deoxygenated samples and lower residuals are for samples equilibrated with 50% air). (B) Profiles of the oxygen

transport parameter for cortical and nuclear lens lipid membranes at 37°C (PCD, phospholipid-cholesterol domain). Approximate localizations of the nitroxide moieties of spin labels are indicated by arrows. Localizations of the nitroxide moieties of Chol analogue spin labels of ASL and CSL in the PCD and the CBD is explained in Sect. 3.5 of Ref. [4].

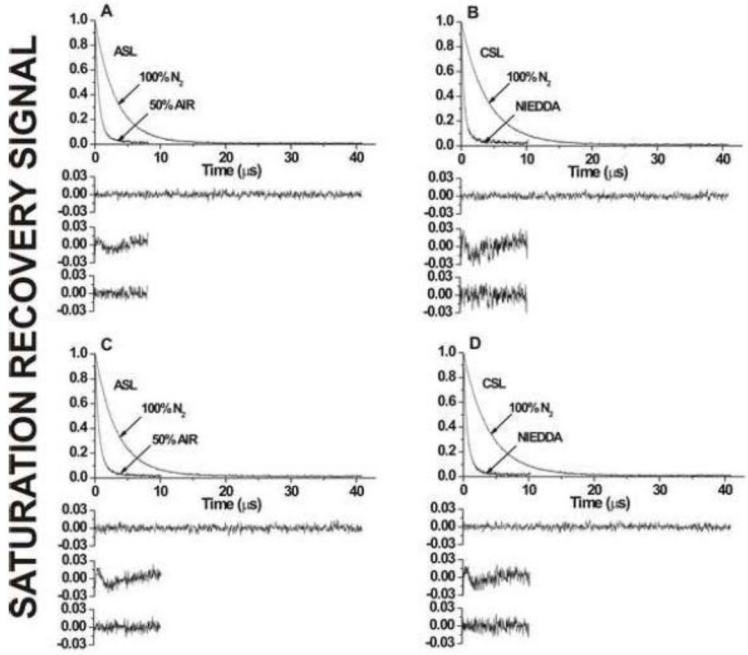

Fig. 4.

SR signals with fitted curves and residuals for (A,C) ASL and (B,D) CSL in (A,B) cortical and (C,D) nuclear lens lipid membranes. Signals were recorded for samples equilibrated with (A–D) 100% nitrogen, (A,C) a gas mixture of 50% air and 50% nitrogen, and (B,D) in the presence of 20 mM NiEDDA. For deoxygenated samples, SR signals were satisfactorily fit to a single-exponential function with time constants of (A) 3.19 ± 0.01 μs, (B) 3.91 ± 0.01 μs, (C) 3.34 ± 0.01 μs, and (D) 3.92 ± 0.01 μs (upper residuals are for single-exponential fit). The SR signal for ASL in the presence of molecular oxygen can be fitted satisfactorily only with double-exponential curves with time constants of (A) 1.34 ± 0.2 and 0.53 ± 0.01 μs and (C) 1.62 ± 0.2 and 0.55 ± 0.01 μs (the middle residual is for single- and the lower residual is for double-exponential fits). The SR signal for CSL in the presence of NiEDDA can be fitted satisfactorily only with double-exponential curves with time constants of (B) 1.54 ± 0.09 and 0.45 ± 0.01 μs and (D) 1.27 ± 0.07 and 0.41 ± 0.01 μs (the middle residual is for single- and the lower residual for double-exponential fits).

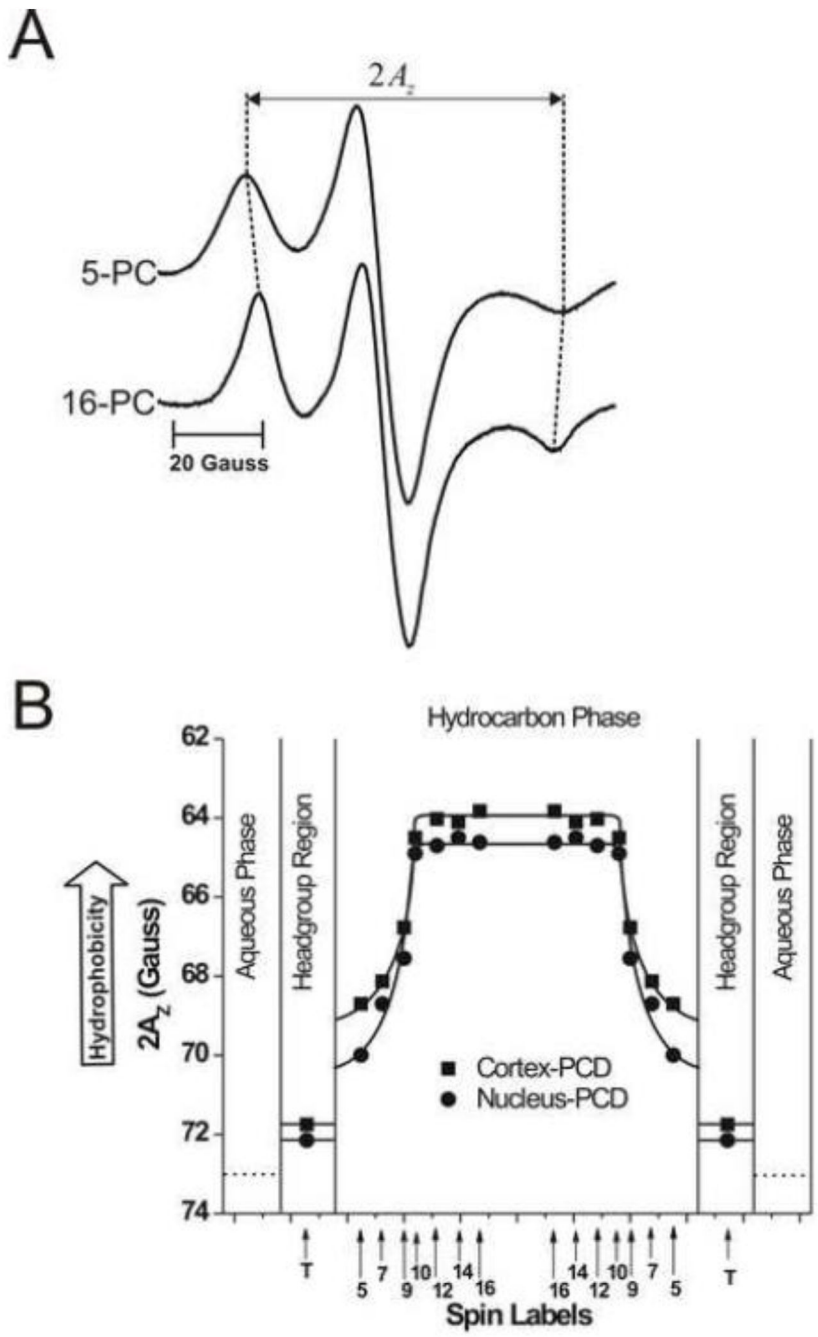

Fig. 5.

(A) Representative EPR spectra of 5- and 16-PC from cortical lens lipid membranes, recorded at −165°C to cancel motional effects. The measured $2A_Z$ value is indicated. (B) Profiles of hydrophobicity ($2A_Z$) for cortical and nuclear lens lipid membranes (PCD, phospholipid-cholesterol domain). Approximate localizations of the nitroxide moieties of spin labels are indicated by arrows.

Table 1

Oxygen transport parameter and NiEDDA accessibility parameter measured with ASL and CSL in domains of the human lens lipid membrane at 37°C

	Oxygen Transport Parameter		NiEDDA Accessibility Parameter	
	ASL (μs^{-1})	CSL (μs^{-1})	ASL (μs^{-1})	CSL (μs^{-1})
Phospholipid–cholesterol domain in cortical membrane	3.11	0.39	0.004	0.39
Cholesterol bilayer domain in cortical membrane	0.78	0.39	0.004	1.97
Phospholipid–cholesterol domain in nuclear membrane	2.99	0.39	0.005	0.53
Cholesterol bilayer domain in nuclear membrane	0.56	0.39	0.005	2.18

Table 2

Permeability coefficients for oxygen (P_M) across domains in human lens lipid membrane and across a water layer of the same thickness as the domain at 37°C

	P_M (cm/s)
Phospholipid–cholesterol domain in cortical membrane	54
Phospholipid–cholesterol domain in nuclear membrane	54
Water layer of the same thickness as the phospholipid–cholesterol domain	72
Cholesterol bilayer domain in cortical membrane	40
Cholesterol bilayer domain in nuclear membrane	32
Water layer of the same thickness as the cholesterol bilayer domain	89